Published July 14, 2014

Journal of Environmental Quality

SPECIAL SECTION

LIVESTOCK GRACEnet

Optimal Sensor Locations for the Backward Lagrangian Stochastic Technique in Measuring Lagoon Gas Emission

Kyoung S. Ro,* Kenneth C. Stone, Melvin H. Johnson, Patrick G. Hunt, Thomas K. Flesch, and Richard W. Todd

This study evaluated the impact of gas concentration and wind sensor locations on the accuracy of measuring gas emission rates from a lagoon environment using the backward Lagrangian stochastic (bLS) inverse-dispersion technique. Path-integrated concentrations (PICs) and three-dimensional (3D) wind vector data were collected at different locations within the lagoon landscape. A floating 45 m × 45 m perforated pipe network on an irrigation pond was used as a synthetic distributed emission source for the controlled release of methane. A total of 961 15-min datasets were collected under different atmospheric stability conditions over a 2-yr period. The PIC location had a significant impact on the accuracy of the bLS technique. The location of the 3D sonic anemometer was generally not a factor for the measured accuracies with the PIC positioned on the downwind berm. The PICs across the middle of the pond consistently produced the lowest accuracy with any of the 3D anemometer locations (<69% accuracy). The PICs located on the downwind berm consistently yielded the best bLS accuracy regardless of whether the 3D sonic anemometer was located on the upwind, side, or downwind berm (accuracies ranged from 79 to 108%). The accuracies of the emission measurements with the berm PIC-berm 3D setting were statistically similar to that found in a more ideal homogeneous grass field. Considering the practical difficulties of setting up equipment and the accuracies associated with various sensor locations, we recommend that wind and concentration sensors be located on the downwind berm.

As a result of biochemical transformation of manures, anaerobic waste lagoons and storage ponds from concentrated animal feeding operations are sources of odor, ammonia, and greenhouse gas emissions (Liang et al., 2002; Vanotti et al., 2009). Accurate assessment of gas emissions from waste lagoons and storage ponds is important for proper planning and management of animal wastes, but the measurement of these gas emissions is challenging. For example, reported emission rates using different measurement methods vary widely (Arogo et al., 2003; Harper, 2005; Harper et al., 2011; Ro et al., 2011). Within these circumstances, the backward Lagrangian stochastic (bLS) inverse-dispersion technique is emerging as a functional micrometeorological method for measuring gas emissions (Flesch et al., 2004; Flesch et al., 2005b; McBain and Desjardins, 2005; Gao et al., 2010; Harper et al., 2010; Ro et al., 2011). In this inverse dispersion technique, the emission rate is calculated from the rise in gas concentration downwind of the emission source. The advantages of the technique are its relatively high accuracy, simplicity, and flexibility in terms of field measurements. From our previous studies in idealized flat terrain, the bLS technique yielded good accuracies (measured emission rate/actual emission rate) of 0.98 ± 0.24 and 0.94 ± 0.24 for single and dual uniformly distributed emission sources, respectively (Ro et al., 2011). However, applying the bLS technique in lagoon settings is complicated because the typical lagoon environment often seemingly violates the bLS's underlying assumption of idealized wind flow over flat and homogenous terrain.

As recommended by the ASAE Engineering Practice 403.3 (ASAE, 1998), many animal waste lagoons are surrounded by vegetative barriers (e.g., trees) to enhance the dispersion and dilution of odors. These barriers complicate the wind flow environment around the lagoon: as the wind moves from the upwind to the downwind side of the lagoon, there is a transition from a highly turbulent zone with low wind speeds, due to the shelter of the trees, to a less turbulent zone with higher wind speeds over the lagoon. One strategy for minimizing the effects

J. Environ. Qual. 43:1111–1118 (2014)
doi:10.2134/jeq2013.05.0163
Received 1 May 2013.
*Corresponding author (kyoung.ro@ars.usda.gov).

K.S. Ro, K.C. Stone, M.H. Johnson, and P.G. Hunt, USDA–ARS Coastal Plains Soil, Water & Plant Research Center, Florence, SC; T.K. Flesch, Univ. of Alberta, Edmonton, AB, Canada; R.W. Todd, USDA-ARS, Conservation & Production Research Lab., Bushland, TX. Mention of trade names or commercial products is solely for the purpose of providing specific information and does not imply recommendation or endorsement by the U.S. Department of Agriculture. Assigned to Associate Editor April Leytem.

Abbreviations: bLS, backward Lagrangian stochastic; 3D, three-dimensional; PIC, path-integrated concentration; S, stable; TDL, open-path tunable diode laser absorption spectrometer; U, unstable; VU, very unstable.

of this localized wind complexity is to move the concentration and wind sensors well downwind of the lagoon and away from the trees and berms to an environment where the wind has re-established a more idealized flow (Flesch et al., 2005a). However, in many situations, especially in the southeastern United States, a clear downwind location for sensors is not available.

We previously reported a relatively good accuracy of 0.88 ± 0.2 for measuring lagoon emission using the bLS technique with a concentration sensor located on the downwind berm (Ro et al., 2013). Other researchers have indicated robustness in simple inverse-dispersion methods applied to environments where the assumptions of idealized wind flow are violated (Wilson et al., 2001; Flesch et al., 2005b; Gao et al., 2010). Thus, some sensor locations in complex environments do not give accurate emission calculations. In all of these cases, it was also possible to accurately infer emissions by avoiding certain sensor locations.

The objective of this study was to identify optimal locations for wind and concentration sensors to accurately measure lagoon gas emissions. This paper reports the results of a study that has significantly expanded the scope of our previous work via a much larger number of datasets (from 104 to 961 datasets) with path-integrated concentrations (PICs) and wind statistics obtained from various locations within the lagoon landscape. Using this expanded dataset, we suggest a set of guidelines to help users identify good and poor locations for wind and concentration sensors within the lagoon boundary.

Materials and Methods

This study was conducted on a rectangular irrigation pond (59 m × 68.5 m) at the USDA–ARS Coastal Plains Soil, Water and Plant Research Center in Florence, South Carolina (34°14.741′ N, 79°48.605′ W). The pond was bordered by pine trees on two sides and by open crop land on the remaining two sides. A small pump house was located along one side. The irrigation pond was filled with ground water from an adjacent well. The berm height above the water ranged from 0.4 to 1.42 m. This site was selected because its surroundings (e.g., tree lines, buildings, and cropland) were similar to typical animal wastewater treatment lagoons in the southeastern United States (Fig. 1). Bales of pine straw (0.25 m × 0.4 m × 0.7 m) were secured midway up the side slopes along the upwind and downwind berm to create an artificial "rough" side slope to simulate an animal manure storage lagoon berm frequently found with heavy vegetation growth in warm climate regions.

A floating perforated pipe network was used as a synthetic distributed lagoon emission source. The floating emission source was constructed of perforated, 1.3-cm schedule 40 polyvinyl chloride pipe assembled into a 45-m^2 grid. The grid was set up with an "I"-shaped manifold connected to a cylinder of compressed methane gas. Laterals were connected at 3-m intervals along the manifold, with 44 1.6-mm holes drilled at 1-m intervals. Circular foam floats were threaded onto each section of the laterals and manifold to float the entire grid on the water surface. The floating grid was secured in the center of the pond so that the laterals were in the northwest-southeast plane.

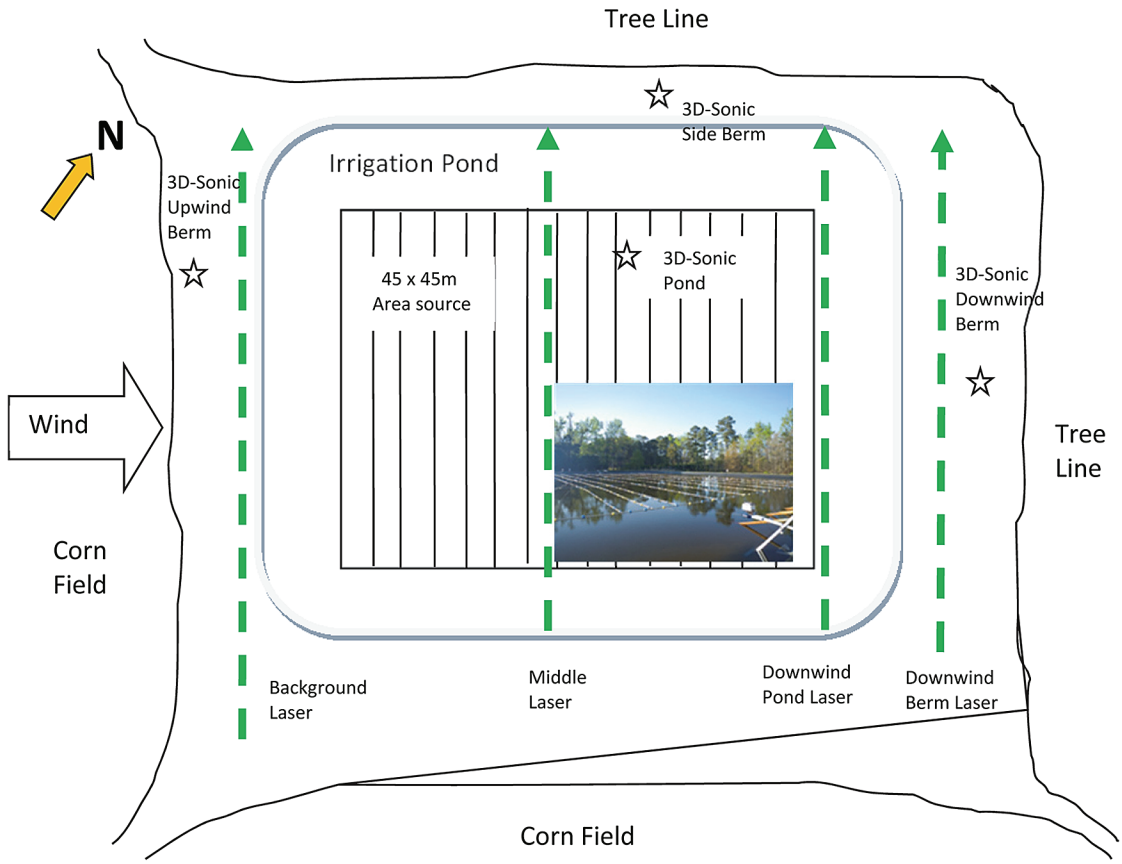

Fig. 1. Irrigation pond layout, floating emission source, and sensor locations.

This 45-m^2 perforated pipe network was designed to provide a uniform discharge flow from all orifices over the entire network. Because the pressure drop through an orifice was about 4 orders of magnitude higher than the pressure drop over the length of manifold for the range of gas flows tested in this study, the manifold acted as an "infinite reservoir" and provided uniform discharge flow distribution. The percent maldistribution, defined as the percentage variation in flow between the first and the last orifices, was <0.001% (Perry and Green, 1997).

Specialized mounting frames were designed to position the instrumentation within the reservoir boundary (Fig. 2). Frames were constructed using lightweight 2-in aluminum square tubing. The frames consisted of a base section designed to maximize the base footprint. The base section was positioned along the edge of the berm and staked to the ground with 0.5-in steel rods. An articulating arm with an adjustable supporting leg extended into the reservoir from the base section. An articulating mounting plate was secured to the end of the support arm. The mounting plate consisted of a 6 in × 12 in aluminum plate supported by 2-in aluminum square tubing. The frames allowed the concentration sensors to be positioned directly over the edge of the water at variable heights. An additional frame was designed to support the 3D sonic anemometer. The anemometer frame was constructed with a similar base section with the addition of weights placed on top of the base. A longer arm section consisted of multiple sections of the 2-in aluminum square tubing, allowing the anemometer position to be well out over the water. A short vertical mast was secured to the end of the arm. The 3D sonic anemometer was mounted on the mast at the desired height.

Pure methane gas (99% CP grade methane, Airgas, Inc.) was used as a test gas, and its true emission rate was calculated from weight loss during experiments. The weight loss of the methane gas cylinder was measured with a 100-kg digital platform scale (Ohaus Champ Platform scale with CW11–2EO indicator). A video camera was used to record the gas flow rate and the weight of the gas cylinder. Change in mass over time and the gas purity were used to calculate the actual emission rate. The methane emission rates for all experiments ranged from 0.3 to 0.7 mg m^{-2} s^{-1}, similar to the methane emission rates from swine anaerobic lagoons (Sharpe and Harper, 1999).

The open-path tunable diode laser absorption spectrometers (TDLs) (GasFinder2.0 for CH_4, Boreal Laser Inc.) and retroreflectors were used to measure PICs along the downwind berm, across the middle of the pond, and along the downwind water's edge of the pond (Fig. 1). The path lengths of these PICs were 63, 55, and 55 m, respectively. The TDLs were set up for a sampling rate of about 1 Hz and had continuous calibration updates every 40 samples using their internal reference cells. In addition, the TDLs were calibrated using an external calibration tube (5 cm i.d. × 6.25 m length) with a standard 30 ppm methane gas before field tests. A more detailed description of the pond and instrumentation can be found in (Ro et al., 2013).

Three-dimensional sonic anemometers (CSAT3, Campbell Scientific, Inc.) were used to measure wind speeds at 20 Hz. The 3D sonic anemometers provided the wind information needed for calculations of friction velocity (u*), Obukhov stability length (L), surface roughness length (z_o), and wind direction (Flesch et al., 2004). During the spring tests (Mar. and Apr. 2011 and 2013),

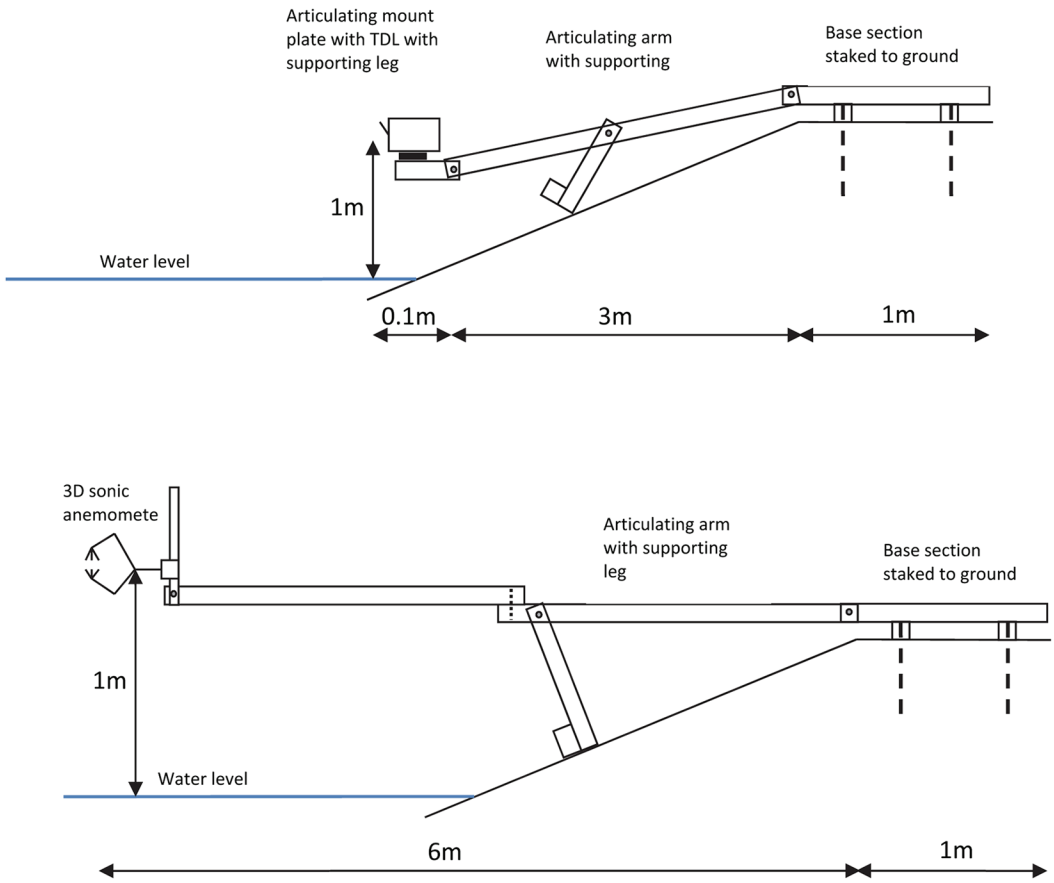

Fig. 2. Schematic diagrams of sensor holders used in this study. TDL, open-path tunable diode laser absorption spectrometer.

the anemometer was installed at the edge of the newly planted corn field approximately 10 m upwind of the pond at a height of 2 m above the ground. The corn field was clear, with little crop growth during spring tests. However, at the start of the summer tests (July, Aug., and Sept. 2011) the corn had grown to over 2 m. Obtaining wind flow data from the upwind anemometer directly facing the tall corn was not feasible; therefore, the anemometer was moved to the side berm or the downwind berm at a height of 2 m above the ground (Fig. 1). This provided a clear fetch of at least 40 m downwind of the corn. After the corn was harvested, additional experiments were conducted to evaluate the impact of surface roughness on the accuracy of the inverse-dispersion technique. These experiments used the wind data obtained from one of two anemometers simultaneously located on the upwind and either the side or the downwind berms of the pond (Sept. 2011 to Feb. 2013). The anemometers were installed facing west.

The PIC data and the 3D wind speeds were averaged at 15-min intervals. For each 15-min period, the background concentrations were subtracted from the downwind concentrations. These net PIC data, along with the averaged wind data from the anemometers, were used as inputs to the Windows-based bLS inverse dispersion computer model, WindTrax 2.0 (Thunder Beach Scientific2008). For each measurement period, the bLS model calculated the upwind trajectory of 50,000 gas "particles" passing through the TDL path and determined the relationship between downwind concentration and the lagoon emission rate. The following data-filtering criteria were used to avoid error-prone observation periods (Ro et al., 2013): (i) footprint coverage (FP) ≥ 20% of the lagoon (based on touchdown coverage in WindTrax); (ii) Obukhov stability length scale, $|L|$, ≥5 m (i.e., to avoid highly stable/unstable atmospheric stratification); and (iii) friction velocity, u^*, ≥0.10 m s^{-1} (changed from ≥0.22 m s^{-1} used in Ro et al. [2013])

The accuracy of the inverse-dispersion technique was calculated as

$$\text{accuracy} = Q_{bLS}/Q \quad [1]$$

where Q is the actual emission rate (g s^{-1}), and Q_{bLS} is the calculated emission rate from the bLS inverse-dispersion technique (g s^{-1}). The central tendency and precision of the accuracy were represented with arithmetic averages and standard deviations (given as ± values in the subsequent accuracy summaries). An unpaired *t* test with Weltch's correction was used for comparing two values. Simple statistical tests (e.g., mean, SD, and *t* tests) were performed using GraphPad Prism 5.04 (GraphPad Software, Inc.). To assess the effects of the sensor locations on accuracy, the data obtained under different atmospheric stability conditions were statistically analyzed in SAS (SAS Institute Inc.) using Proc GLIMMIX.

Results and Discussion

For convenience, the PICs measured from the TDL at the middle of the pond at 1 m above the water surface are referred to as "middle PIC," the PICs from the TDL at the downwind edge of the pond at 1 m above water surface are referred to as "lower PIC," the PICs obtained from the TDL at the downwind berm are referred to as "berm PIC," the 3D sonic anemometer positioned on the upwind berm of the pond is referred to as "upwind 3D," the 3D sonic anemometer positioned on the side berm of the pond is referred to as "side 3D," the 3D sonic anemometer positioned on the downwind berm of the pond is referred to as "berm 3D," and the 3D sonic anemometer 1 m above water surface of the pond and 6 m from the berm is referred to as "pond 3D."

Ro et al. (2013) used the friction velocity criterion of $u^* \geq 0.22$ m s^{-1} to filter their berm PIC datasets. However, evaluation of this study's comprehensive datasets, including additional pond 3D, middle and lower PIC datasets suggested that we could lower the friction velocity criterion to $u^* \geq 0.1$ m s^{-1} without sacrificing accuracy (Table 1). Much of highly scattered data were eliminated by filtering the data with the FP ≥ 20% criterion. This FP criterion significantly reduced the standard deviation from 3.4 to 0.41 with only a 1% reduction in the number of datasets. The standard deviation was further decreased from 0.41 to 0.33 when an additional criterion of $|L| \geq 5$ m was applied. The additional criterion of $u^* \geq 0.1$ m s^{-1} did not improve the accuracy or the standard deviation while losing only one dataset. It appeared as if these two criteria ($|L|$ and u^*) were essentially equivalent in our case (reflecting the functional relationship between L and u^*). Therefore, we selected the new data criteria (FP ≥ 20%, $|L| \geq 5$ m, $u^* \geq 0.1$ m s^{-1}) to avoid the error-prone datasets. These new data criteria resulted in an approximately 15% reduction in the total number of datasets.

Table 2 shows the summary of relative accuracies of all experimental runs consisting of 961 datasets. The datasets were also subdivided into different atmospheric stability conditions (Tables 3–5). We followed Seinfeld (1986) and categorized the atmosphere as "very unstable (VU)," "unstable (U)," "neutral (N)," "stable (S)," or "very stable (VS)" based on the Monin-Obukhov length values of -100 m $< L < 0$, -10^5 m $\leq L \leq -100$ m, $|L| > 10^5$ m, 10 m $\leq L \leq 10^5$ m, and $0 < L < 10$ m, respectively. Seventy percent of the 961 datasets were obtained under VU conditions, and 11, 17, and 2% of the datasets were obtained under U, S, and VS atmospheric conditions, respectively.

The overall average accuracy (Q_{bLS}/Q) was 0.76 ± 0.33. The means of Q_{bLS}/Q for PIC locations across all 3D sonic locations ranged from 0.41 to 1.18, 0.0 to 1.75, and 0.28 to 0.96 for VU, U, and S atmospheric conditions, respectively. There was significant variability in accuracy depending on the location of the TDL

Table 1. Accuracy, standard deviation, and number of datasets with various data filtering criteria.

	All	FP† ≥ 20%	FP ≥ 20%, $\|L\|$‡ ≥ 5 m	FP ≥ 20%, $\|L\|$ ≥ 5 m, u^*§ ≥ 0.1 m s^{-1}	FP ≥ 20%, $\|L\|$ ≥ 5 m, u^* ≥ 0.22 m s^{-1}
Mean (SD)	0.94 (3.4)	0.79 (0.41)	0.76 (0.33)	0.76 (0.33)	0.75 (0.31)
Number of datasets	1129	1115	962	961	747

† Footprint coverage.

‡ Obukhov stability length.

§ Friction velocity.

Table 2. Accuracies of the backward Lagrangian stochastic technique using sensors at various locations under all atmospheric stability conditions.

3D sonic anemometer location	PIC† location	Berm surface roughness	Temp.	Wind speed	Q_{bLS}/Q‡	No. of datasets
			°C	m s^{-1}		
Upwind 3D	middle	smooth	23.4 ± 4.7	4.8 ± 2.4	0.69 ± 0.30	41
		rough	15.5 ± 1.8	4.2 ± 1.6	0.43 ± 0.25	32
	lower	smooth	24.0 ± 4.3	5.1 ± 2.2	1.06 ± 0.48	38
		rough	15.8 ± 1.9	3.8 ± 1.8	0.73 ± 0.23	37
	berm§	smooth	23.7 ± 4.6	5.0 ± 2.3	1.04 ± 0.38	39
		rough	17.5 ± 4.2	4.3 ± 1.4	0.90 ± 0.11	40
					0.82 ± 0.38	227
side 3D	middle	smooth	19.9 ± 2.9	4.2 ± 1.1	0.37 ± 0.12	30
		rough	32.5 ± 1.7	2.5 ± 0.8	0.68 ± 0.19	45
	lower	smooth	20.1 ± 2.6	4.7 ± 1.3	0.80 ± 0.33	39
		rough	32.5 ± 1.8	2.6 ± 0.8	0.74 ± 0.19	42
	berm*	smooth	22.5 ± 5.7	4.1 ± 1.1	1.08 ± 0.33	38
		rough	32.1 ± 2.1	2.8 ± 0.8	0.79 ± 0.23	51
					0.76 ± 0.31	245
berm 3D	middle	smooth	20.3 ± 2.6	4.2 ± 1.2	0.49 ± 0.13	31
		rough	15.7 ± 1.9	4.1 ± 1.6	0.45 ± 0.22	33
	lower	smooth	20.4 ± 2.3	4.6 ± 1.4	0.83 ± 0.35	40
		rough	16.1 ± 2.0	3.6 ± 1.8	0.74 ± 0.42	40
	berm§	smooth	22.3 ± 4.4	4.2 ± 1.1	0.99 ± 0.19	40
		rough	17.6 ± 4.2	4.3 ± 1.4	0.92 ± 0.32	40
					0.76 ± 0.36	224
Pond 3D	middle	smooth	23.3 ± 4.5	4.8 ± 2.4	0.64 ± 0.22	41
		rough	32.6 ± 1.6	2.4 ± 0.9	0.67 ± 0.14	51
	lower	smooth	24.1 ± 3.9	5.2 ± 2.2	1.02 ± 0.51	37
		rough	32.6 ± 1.8	2.4 ± 0.9	0.65 ± 0.18	49
	berm	smooth	24.3 ± 4.0	5.2 ± 2.1	0.77 ± 0.22	37
		rough	32.6 ± 1.7	2.5 ± 0.9	0.60 ± 0.19	50
					0.71 ± 0.29	265
Overall					0.76 ± 0.33	961

† Path-integrated concentration.

‡ Accuracy of the inverse-dispersion technique, where Q is the actual emission rate (g s^{-1}), and Q_{bLS} is the calculated emission rate from the backward Lagrangian stochastic inverse-dispersion technique (g s^{-1}).

§ Old datasets (n = 104) (Ro et al., 2013) were combined with the new data from this study.

Table 3. Mean accuracies statistical analysis of backward Lagrangian stochastic technique using sensors at various locations for the very unstable atmospheric stability conditions.

Berm surface roughness	3D sonic anemometer location	PIC† location			3D sonic mean
		Berm	Lower	Middle	
			Q_{bls}/Q‡		
Rough	berm3D	1.00 ± 0.44a§	0.67 ± 0.55b	0.41 ± 0.25b	0.70 ± 0.50ab¶
	pond3D	0.60 ± 0.20b	0.65 ± 0.12ab	0.68 ± 0.14a	0.66 ± 0.18b
	side3D	0.78 ± 0.22a	0.74 ± 0.18ab	0.68 ± 0.19b	0.74 ± 0.20a
	upwind3D	0.91 ± 0.12a	0.71 ± 0.26b	0.47 ± 0.20c	0.71 ± 0.26ab
	PIC location mean	0.78 ± 0.28a	0.69 ± 0.29b	0.61 ± 0.21c	0.70 ± 0.27
smooth	berm3D	1.09 ± 0.19a	1.00 ± 0.19a	0.49 ± 0.15b	0.88 ± 0.32b
	pond3D	0.84 ± 0.26b	1.18 ± 0.63a	0.70 ± 0.11b	0.89 ± 0.42b
	side3D	1.14 ± 0.35a	0.98 ± 0.16b	0.41 ± 0.11c	0.87 ± 0.39b
	upwind3D	1.11 ± 0.44a	1.18 ± 0.56a	0.80 ± 0.29b	1.02 ± 0.46a
	PIC Location Mean	1.07 ± 0.34a	1.08 ± 0.42a	0.61 ± 0.25b	0.92 ± 0.41

† Path integrated concentration.

‡ Accuracy of the inverse-dispersion technique, where Q is the actual emission rate (g s^{-1}), and Q_{bLS} is the calculated emission rate from the backward Lagrangian stochastic inverse-dispersion technique (g s^{-1}).

§ Row means followed by the same letter are not significantly different at the p = 0.05 level.

¶ Column means for the 3D sonic anemometer location followed by the same letter are not significantly different at the p = 0.05 level.

used in the bLS calculation. The berm PIC and lower PIC for all 3D sonic anemometer positions produced significantly better accuracy than the middle PIC for all atmospheric and berm roughness conditions. The location of the 3D sonic anemometer was generally not a factor for the measured accuracies with the PIC positioned on the downwind berm under all berm surface and atmospheric stability conditions. The berm 3D as a control did not produce a significantly different accuracy compared with upwind 3D, side 3D, or pond 3D (Dunnett's multiple comparison test, $P > 0.05$). For smooth berm surface under VU and U atmospheric stability, equivalently excellent accuracy was produced by berm PIC and lower PIC for all 3D sonic anemometer positions.

It was interesting to observe the consistently poor accuracies associated with the middle PIC for all sonic locations, berm surface, and atmospheric stability conditions. We conjectured that the middle PIC was above the gas plume constricted by the shallow lagoon boundary layer. Because all our sonic locations were also above this layer, the transport of gas from the lagoon surface to the PIC was not well described by the flow measured at any of the sonic locations. To gain further insight on the gas plume location, we compared the middle PICs and lower PICs (Fig. 3). During the periods when the middle PIC pond 3D produced relatively good results with less than ±30% errors (i.e., $0.7 \le Q_{bLS}/Q \le 1.3$), the average CH_4 concentration of the middle PICs were significantly higher than that of the lower PICs ($P = 0.002$). However, during the periods of poor results (i.e., $Q_{bLS}/Q < 0.7$ or > 1.3), the average CH_4 concentration of the middle PICs was not significantly different from that of the lower PICs ($P = 0.125$). Therefore, we reasoned that the middle PIC might have missed the gas plume during the low-accuracy

Table 4. Mean accuracies statistical analysis of backward Lagrangian stochastic technique using sensors at various locations for the unstable atmospheric conditions.

Berm surface roughness	3D sonic anemometer location	PIC† location			3D sonic mean
		Berm	Lower	Middle	
		Q_{bls}/Q‡			
Rough	berm3D	0.85 ± 0.08a§	0.85 ± 0.07a	0.55 ± 0.16b	0.75 ± 0.18a¶
	pond3D	0.63 ± 0.10a	0.64 ± 0.12a	0.51 ± 0.13a	0.59 ± 0.12b
	side3D	1.10			1.10.§
	upwind	0.91 ± 0.17a	0.83 ± 0.11a	0.00 ± 0.00b	0.63 ± 0.44b
	PIC location mean	0.84 ± 0.15a	0.80 ± 0.12a	0.46 ± 0.24 b	0.71 ± 0.24
Smooth	berm3D	0.90 ± 0.11b	1.06 ± 0.08a	0.48 ± 0.09c	0.81 ± 0.27b
	pond3D	0.60	1.08	1.75.	1.14 ± 0.58#
	side3D	1.00 ± 0.07a	1.02 ± 0.10a	0.30 ± 0.02b	0.77 ± 0.37bc
	upwind	0.91 ± 0.12a	0.87 ± 0.19a	0.42 ± 0.10b	0.73 ± 0.26c
	PIC location mean	0.90 ± 0.13a	0.96 ± 0.17a	0.49 ± 0.17b	0.78 ± 0.27

† Path integrated concentration.

‡ Accuracy of the inverse-dispersion technique, where Q is the actual emission rate (g s^{-1}), and Q_{bLS} is the calculated emission rate from the backward Lagrangian stochastic inverse-dispersion technique (g s^{-1}).

§ Row means followed by the same letter are not significantly different at the $p = 0.05$ level.

¶ Column means for the 3D Sonic Anemometer Location followed by the same letter are not significantly different at the $p = 0.05$ level.

Only one observation was measured for the unstable atmospheric condition, and it was not included in the statistical analysis.

Table 5. Mean accuracies statistical analysis of backward Lagrangian stochastic technique using sensors at various locations for the stable atmospheric conditions.

Berm surface roughness	3D sonic anemometer location	PIC† location			3D sonic mean
		Berm	Lower	Middle	
		Q_{bls}/Q‡			
Rough	berm3D	0.83 ± 0.12a§	0.85 ± 0.07a	0.40 ± 0.22b	0.71 ± 0.25a¶
	pond3D				
	side3D				
	upwind	0.87 ± 0.07a	0.81 ± 0.07a	0.43 ± 0.35b	0.70 ± 0.28a
	PIC location mean	0.84 ± 0.10a	0.83 ± 0.07a	0.41 ± 0.27b	0.71 ± 0.26
Smooth	berm3D	0.88 ± 0.08a	0.50 ± 0.37b	0.49 ± 0.16b	0.62 ± 0.32bc
	pond3D	0.79 ± 0.12a	0.96 ± 0.44a	0.56 ± 0.10b	0.76 ± 0.31a
	side3D	0.86 ± 0.18a	0.48 ± 0.33b	0.28 ± 0.11b	0.53 ± 0.33c
	upwind	0.86 ± 0.16a	0.78 ± 0.09ab	0.62 ± 0.05b	0.75 ± 0.14ab
	PIC location mean	0.83 ± 0.13a	0.69 ± 0.44b	0.49 ± 0.32c	0.68 ± 0.32

† Path integrated concentration.

‡ Accuracy of the inverse-dispersion technique, where Q is the actual emission rate (g s^{-1}), and Q_{bLS} is the calculated emission rate from the backward Lagrangian stochastic inverse-dispersion technique (g s^{-1}).

§ Row means followed by the same letter are not significantly different at the $p = 0.05$ level.

¶ Column means for the 3D sonic anemometer location followed by the same letter are not significantly different at the $p = 0.05$ level.

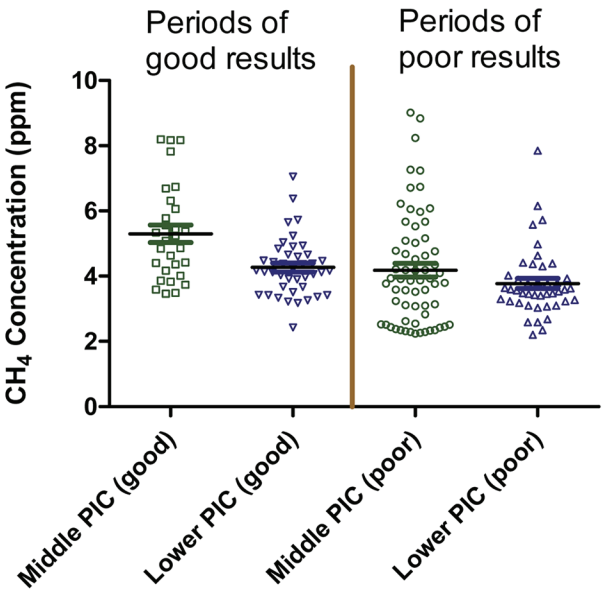

Fig. 3. Comparison of middle path-integrated concentrations (PICs) and lower PICs.

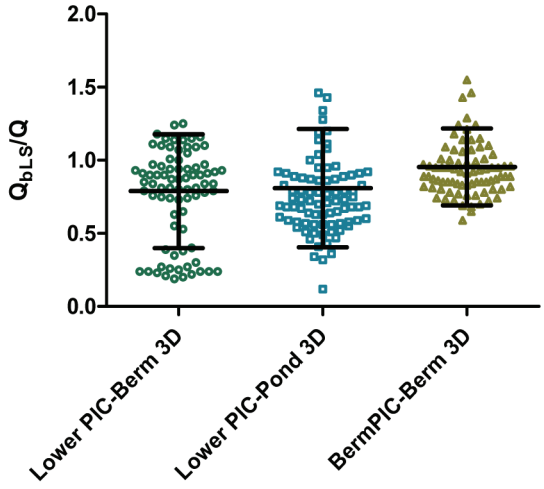

Fig. 4. Comparison of accuracies associated with instruments positioned above water surface and on the downwind berm. PIC, path-integrated concentration; Q_{bLS}/Q, accuracy of the inverse-dispersion technique, where Q is the actual emission rate (g s^{-1}), and Q_{bLS} is the calculated emission rate from the backward Lagrangian stochastic inverse-dispersion technique (g s^{-1}).

periods. However, without the aid of a 3D flow model to evaluate this hypothesis, we can only speculate at this time.

Another interesting observation was that the combined accuracy for smooth and rough berm surfaces of the lower PIC pond 3D (0.79 ± 0.39) was not significantly different from that of the lower PIC berm 3D (0.81 ± 0.40) (Fig. 4). The lower PIC-pond 3D configuration should yield better emission measurements than the berm PIC-pond 3D due to close proximity of the sensors to the lagoon's internal boundary layer. However, we speculated that the 3D sonic anemometer positioned 1 m above the water surface (i.e., pond 3D) could miss some of the turbulence because the sonic measurement path length might be large relative to the smaller size of the eddies close to the water surface. The turbulence could be studied with spectral analyses of the sonic signals, but such systematic study is intensive and beyond the scope of this paper. We assumed that the signal loss was relatively small. For a height of 1 m, the errors in heat and momentum fluxes caused by frequency attenuation will be <5%, assuming ideal flat terrain turbulent spectra (Horst, 1997; Massman, 2000).

The berm PIC–berm 3D with both sensors away from the lagoon's internal boundary layer yielded the best combined accuracy of 0.95 ± 0.26 (Fig. 4). This finding appeared to argue against the ideas of some researchers (Wilson et al., 2001; Flesch et al., 2007; McGinn et al., 2008) of avoiding the complex wind flow around lagoon borders, which is influenced by the aerodynamics of the lagoon surface, the berms, and the surrounding landscape. In light of this, it is not clear why we found the opposite to be the case. Perhaps our study pond is too small to establish a stable lagoon boundary layer over the water surface, or the berm height may not be high enough to create significant wind complexity around the pond border. Future work on spectral analyses of sonic anemometer data collected on the water surface and on the berms of various lagoons with different sizes and surroundings is needed to elucidate the reasons for this finding. Nevertheless, this was a fortunate finding because it would require considerably more effort to install sensors directly over the water surface, especially for animal waste lagoons.

We also compared the accuracies of the berm PIC–berm 3D with those obtained from a more ideal terrain setting (i.e., homogeneous flat grass field without the land-to-water transitions) (Ro et al., 2011). The terrain was covered with short Bermudagrass (<0.1 m tall) at the time of the study. A 27-m^2 grid of 1.3-cm perforated polyvinyl chloride pipe similar to current floating pipe network was used as a synthetic emission source with a known emission rate. The instruments to obtain wind statistics and PICs were the same as that used in this study. Figure 5 shows that the sensor locations were similar to the current pond study (i.e., wind and concentration sensors were positioned along the downwind side of the synthetic emission source; data taken on 26 Feb. 2009 using M2 or M3 of Ro et al. [2011]). There were no significant differences among bLS accuracies for the pond emission or for the distributed land emission (P = 0.20) (Table 6). It appeared that the land–water complexity, berm, and the surrounding trees did not play a significant role for pond emission when the berm 3D and berm

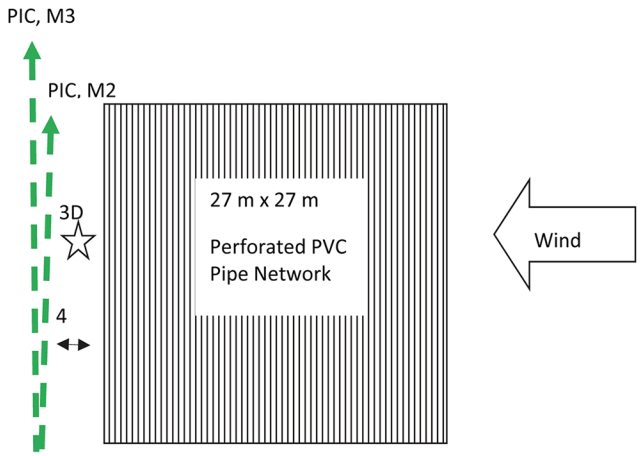

Fig. 5. Layout of synthetic land emission source, path-integrated concentration (PIC), and three-dimensional sonic anemometer. M2 and M3 are as described by Ro et al. [2011]).

Table 6. Comparison of backward Lagrangian stochastic accuracies for pond and land emission sources.

Site condition	3D sonic anemometer location	PIC† location	Berm surface	Atmospheric stability	Q_{bLS}/Q‡	No. of datasets
Pond	downwind berm	downwind berm	smooth	very unstable	0.99 ± 0.19	40
Pond	downwind berm	downwind berm	rough	very unstable	0.91 ± 0.31	40
Land	downwind emission source	downwind emission source	grass <0.1 m	very unstable	0.87 ± 0.14	12

† Path-integrated concentration.

‡ Accuracy of the inverse-dispersion technique, where Q is the actual emission rate (g s^{-1}), and Q_{bLS} is the calculated emission rate from the backward Lagrangian stochastic inverse-dispersion technique (g s^{-1}).

PICs were used in the bLS calculation. This is a significant, and again fortunate, finding because installation of sensors on the berm is much simpler and requires less time and costs less than installation at other locations directly above the water surface.

Conclusions

This study compared the accuracies of the bLS technique in measuring lagoon emissions using wind and concentration sensors located at various positions around the lagoon. The bLS accuracy was sensitive to the location of the PIC concentration sensor. The most accurate measurements occurred when the PIC was located on the downwind berm regardless of atmospheric stratification, berm roughness, or the location of sonic anemometer. For this PIC location, the bLS accuracies ranged from 79 to 108% with the sonic anemometer located on any side of the berm. The least accurate configuration had the PIC positioned over the middle of the lagoon for all sonic anemometer locations. These are very favorable results considering the practical difficulties in setting up equipment in the locations other than on berm. The accuracy of the emission calculations in this scenario is similar to that found in more ideal cases involving a distributed emission source on a homogeneous, flat, grass-covered terrain. Based on this rigorous tracer study, we recommend that the bLS technique with the optimal sensor location (both sensors located on downwind berm) is convenient and accurate enough to measure lagoon emissions.

Acknowledgments

The authors thank Brian Crenna of the Thunder Beach Scientific, Ray Winans, Joe Millen, William Brigman, and Dr. Phil Bauer of the USDA-ARS Coastal Plains Soil, Water & Plant Research Center, Florence, SC, for technical support. This research is part of the USDA-ARS National Programs 211 Water Availability and Watershed Management and 214 Agricultural and Industrial Byproduct Utilization.

References

Arogo, J., P.W. Westerman, and A.J. Heber. 2003. A review of ammonia emissions from confined swine feeding operations. Trans. ASABE 46:805–817.

ASAE. 1998. Engineering practices: 403.3. Design of anaerobic lagoons for animal waste management. ASAE, St. Joseph, MI.

Flesch, T.K., J.D. Wilson, and L.A. Harper. 2005a. Deducing ground-to-air emissions from observed trace gas concentrtions: A field trial with wind disturbance. J. Appl. Meteorol. 44:475–484. doi:10.1175/JAM2214.1

Flesch, T.K., J.D. Wilson, L.A. Harper, and P.C. Brian. 2005b. Estimating gas emissions from a farm with an inverse-despersion technique. Atmos. Environ. 39:4863–4874. doi:10.1016/j.atmosenv.2005.04.032

Flesch, T.K., J.D. Wilson, L.A. Harper, B.P. Crenna, and R.R. Sharpe. 2004. Deducing ground-to-air emissions from observed trace gas concentrations: A field trial. J. Appl. Meteorol. 43:487–502. doi:10.1175/1520-0450(2004)043<0487:DGEFOT>2.0.CO;2

Flesch, T.K., J.D. Wilson, L.A. Harper, R.W. Todd, and N.A. Cole. 2007. Determining ammonia emissions from a cattle feedlot with an inverse dispersion technique. Agric. For. Meteorol. 144:139–155. doi:10.1016/j.agrformet.2007.02.006

Gao, Z., R.L. Desjardins, and T.K. Flesch. 2010. Assessment of the uncertainty of using an inverse-dispersion technique to measure methane emissions from animals in a barn and in a small pen. Atmos. Environ. 44:3128–3134. doi:10.1016/j.atmosenv.2010.05.032

Harper, L.A. 2005. Micrometerological measurements in agricultural systems. In: J.L. Hatfield and J.M. Baker, editors, Micrometeorology in agricultural systems. Agron. Monogr. 47. ASA, CSSA, SSSA, Madison, WI.

Harper, L.A., O.T. Denmead, and T.K. Flesch. 2011. Micrometeorological techniques for measurement of greenhouse gas emissions from ruminant animal production. Anim. Feed Sci. Technol. 166–167:227–239. doi:10.1016/j.anifeedsci.2011.04.013

Harper, L.A., T.K. Flesch, K.H. Weaver, and J.D. Wilson. 2010. The effect of biofuel production on swine farm ammonia and methane emissions. J. Environ. Qual. 39:1984–1992. doi:10.2134/jeq2010.0172

Horst, T.W. 1997. A simple formula for attenuation of eddy fluxes measured with first-order response scalar sensors. Boundary-Layer Meteorol. 82:219–233. doi:10.1023/A:1000229130034

Liang, Z.S., P.W. Westerman, and J. Arogo. 2002. Modeling ammonia emission from swine anaerobic lagoons. Trans. ASABE 45:787–798.

Massman, W.J. 2000. A simple method for estimating frequency response corrections for eddy covariance systems. Agric. For. Meteorol. 104:185–198. doi:10.1016/S0168-1923(00)00164-7

McBain, M.C., and R.L. Desjardins. 2005. The evaluation of a backward Lagrangian stochastic (bLS) model to estimate greenhouse gas emissions from agricultural sources using a synthetic tracer source. Agric. For. Meteorol. 135:61–72. doi:10.1016/j.agrformet.2005.10.003

McGinn, S.M., T. Coats, T.K. Flesch, and B.P. Crenna. 2008. Ammnia emissions from dairy cow manure stored in a lagoon over summer. Can. J. Soil Sci. 88:611–615. doi:10.4141/CJSS08002

Perry, R.H., and D.W. Green. 1997. Perry's chemical engineers' handbook. 7th ed. McGraw-Hill, New York.

Ro, K.S., M.H. Johnson, P.G. Hunt, and T.K. Flesch. 2011. Measuring trace gas emission from multi-distributed sources using vertical radial plume mapping (VRPM) and backward Lagrangian stochastic (bLS) techniques. Atmosphere (Toronto) 2:553–566. doi:10.3390/atmos2030553

Ro, K.S., M.H. Johnson, K.C. Stone, P.G. Hunt, T.K. Flesch, and R.W. Todd. 2013. Measuring gas emissions from animal waste lagoons with an inverse-dispersion technique. Atmos. Environ. 66:101–106. doi:10.1016/j.atmosenv.2012.02.059

Seinfeld, J.H. 1986. Atmospheric chemistry and physics of air pollution. John Wiley & Sons, New York.

Sharpe, R.R., and L.A. Harper. 1999. Methane emissions from an anaerobic swine lagoon. Atmos. Environ. 33:3627–3633. doi:10.1016/S1352-2310(99)00104-1

Thunder Beach Scientific. 2008. http://www.thunderbeachscientific.com/ (accessed 3 Oct. 2008).

Vanotti, M.B., A.A. Szogi, P.D. Millner, and J.H. Loughrin. 2009. Development of a second-generation environmentally superior technology for treatment of swine manure in the USA. Bioresour. Technol. 100:5406–5416. doi:10.1016/j.biortech.2009.02.019

Wilson, J.D., T.K. Flesch, and L.A. Harper. 2001. Micro-meteorological methods for estimating surface exchange with a disturbed windflow. Agric. For. Meteorol. 107:207–225. doi:10.1016/S0168-1923(00)00238-0